water

MDPI

Article

Cooling–Heating Phase Behavior of Hypersaline Culture Media Studied by DSC and Cryomicroscopy

Olena Bobrova [1,2,*], Nadiia Chernobai [1], Nadiia Shevchenko [1], Viktor Husak [3] and Alexander Shyichuk [4,5,*]

[1] Laboratory of Phytocryobiology, Institute for Problems of Cryobiology and Cryomedicine NAS of Ukraine, Pereyaslavska 23, 61015 Kharkiv, Ukraine; nadiiachernobai@cryonas.org.ua (N.C.); n.o.shevchenko@nas.gov.ua (N.S.)
[2] Division of Genetics and Plant Breeding, Czech Agrifood Research Center, Drnovska 507/73, 16100 Prague, Czech Republic
[3] Department of Biochemistry and Biotechnology, Vasyl Stefanyk Carpathian National University, Shevchenka 57, 76018 Ivano-Frankivsk, Ukraine; viktor.husak@cnu.edu.ua
[4] Educational and Scientific Center of Materials Science and Nanotechnology, Vasyl Stefanyk Carpathian National University, 76018 Ivano-Frankivsk, Ukraine
[5] Faculty of Chemical Technology and Engineering, Bydgoszcz University of Science and Technology, Seminaryjna 3, 85-326 Bydgoszcz, Poland
* Correspondence: olena.bobrova@carc.cz (O.B.); szyjczuk@pbs.edu.pl (A.S.)

Abstract

Hypersaline culture media used for cultivation of *Dunaliella salina* represent complex multicomponent aqueous systems whose cooling–heating phase behavior remains insufficiently characterized. In this study, the thermal transitions of two biologically relevant hypersaline media (Artari and Ramaraj) were investigated using differential scanning calorimetry (DSC) and cryomicroscopy. The media were examined at NaCl concentrations of 1.5, 2.0, and 4.0 M, corresponding to moderate to highly concentrated brine conditions comparable to natural salt lakes and evaporative basins. DSC analysis revealed pronounced salinity-dependent suppression of ice crystallization and modification of melting transitions relative to classical NaCl–water systems. Increased NaCl concentration reduced recrystallization during heating and shifted peak temperatures, indicating kinetic and compositional effects in the unfrozen fraction. Rapid cooling promoted formation of partially amorphous phases, consistent with limited vitrification in highly concentrated media. Cryomicroscopy directly confirmed changes in ice morphology, nucleation density, and crystal growth dynamics under varying salinity and thermal histories. The combined calorimetric and microscopic approach demonstrates that complete hypersaline cultivation media exhibit phase behavior that cannot be fully extrapolated from simplified binary systems. These findings provide new insight into the physicochemical stability of multicomponent brines during cooling and highlight the critical role of salinity and thermal history in controlling crystallization pathways in hypersaline aqueous environments.

Keywords: saline culture media; phase transitions; ice crystallization; glassy state; differential scanning calorimetry; cryomicroscopy; cooling–heating cycles; hypersaline solutions; water–salt systems

Check for updates

Academic Editor: Chi-Wang Li

Received: 25 January 2026
Revised: 10 March 2026
Accepted: 19 March 2026
Published: 21 March 2026

Copyright: © 2026 by the authors. Licensee MDPI, Basel, Switzerland. This article is an open access article distributed under the terms and conditions of the Creative Commons Attribution (CC BY) license.

1. Introduction

Hypersaline aquatic environments, including salt lakes, solar salterns, evaporative basins, and continental brines, represent extreme ecosystems characterized by high ionic

strength and strong physicochemical variability [1,2]. Such environments frequently experience pronounced daily and seasonal temperature fluctuations and, in temperate regions, recurrent freeze–thaw cycles that further modify brine chemistry and microstructure. These systems host diverse communities of halophilic and halotolerant microorganisms, including microalgae (e.g., *Dunaliella* spp.), haloarchaea, cyanobacteria, and invertebrates such as *Artemia* [1,2]. Among them, *Dunaliella salina* has become a model organism for investigating salt adaptation and is widely exploited in biotechnology due to its ability to grow across an exceptionally broad salinity range [3–7].

The physiological plasticity of *Dunaliella* under varying salinity has been extensively studied, including osmotic regulation, glycerol accumulation, and carotenoid production [4,8,9]. Culture medium composition strongly influences growth kinetics and metabolite production [10,11], underscoring the importance of physicochemical properties of hypersaline media in both laboratory and industrial applications.

In both natural and engineered hypersaline systems, organisms experience not only osmotic stress but also physicochemical changes associated with cooling and warming. Subzero temperatures induce ice crystallization, eutectic phase formation, and progressive solute exclusion into increasingly concentrated brine channels. Freezing-point depression in electrolyte solutions is well documented experimentally and thermodynamically [12], and water activity is a key determinant of ice nucleation in saline systems [13]. Ice nucleation kinetics in NaCl solutions can shift from single-step to multi-step mechanisms depending on thermodynamic conditions [14]. Confinement and high solute concentration further modify crystallization pathways [15]. In this context, thermal history refers to the sequence of cooling and heating conditions experienced by the solution, including cooling rate, minimum temperature reached, and subsequent warming rate, which together influence nucleation and recrystallization processes.

These processes alter local ionic strength, pH, and microstructure, thereby modifying the physicochemical microenvironment surrounding cells. Recrystallization during warming plays a critical role in the structural evolution of frozen systems and is strongly dependent on solute mobility and composition [16,17]. In cryobiological systems, such processes are directly linked to mechanical and osmotic stress on cells [18,19]. Moreover, hypersaline culture media used in laboratory and industrial settings may undergo cooling during storage, transport, or cryopreservation procedures, making their thermal behavior practically relevant [20,21].

Beyond terrestrial systems, concentrated saline solutions with depressed freezing points are increasingly investigated as analogs of extraterrestrial cryobrines in planetary science and astrobiology [22]. Highly concentrated perchlorate and chloride brines can remain liquid at subzero temperatures and may form supercooled or glassy states under appropriate conditions [22]. Understanding crystallization pathways, eutectic transitions, and potential non-crystalline or kinetically constrained phases in multicomponent saline solutions is therefore of broader physicochemical and planetary relevance.

A systematic investigation of cooling–heating phase transitions in these complex saline formulations is therefore important for several interconnected reasons. First, it provides insight into the physicochemical microenvironments formed during freezing in hypersaline ecosystems. Second, it informs the stability and thermal handling of concentrated culture media in biotechnological applications. Third, it contributes to cryobiological knowledge relevant to the preservation and transport of halophilic microorganisms. Finally, multicomponent hypersaline media serve as experimentally accessible model systems for studying concentrated cryobrines under controlled laboratory conditions.

However, experimental studies that integrate calorimetric characterization with direct visualization of microstructural evolution during freezing and melting in complete

hypersaline culture media are largely absent. In particular, correlations between differential scanning calorimetry (DSC) thermograms and real-time microscopic observation of ice nucleation, eutectic formation, recrystallization, and potential amorphous phases have not been systematically explored for biologically relevant saline formulations.

The present study addresses this gap by investigating the cooling–heating phase behavior of two widely used hypersaline culture media compositions (Artari and Ramaraj variants) using a combined DSC and cryomicroscopy approach. These media were selected because they represent realistic multicomponent cultivation systems for halophilic microalgae and differ in overall salinity and ionic complexity, thereby enabling evaluation of composition- and salinity-dependent phase behavior within biologically meaningful frameworks.

By integrating calorimetric measurements with direct microscopic visualization, this work aims to:

- Identify and assign thermal events corresponding to ice crystallization, eutectic melting, and recrystallization;
- Examine the influence of salinity level and medium composition on nucleation temperature, melting-point depression, and kinetic effects;
- Characterize microstructural evolution during cooling and warming cycles;
- Assess whether the phase behavior of complex hypersaline culture media differs from that expected for simplified NaCl–water systems reported in the literature.

To our knowledge, this is the first systematic study combining DSC and cryomicroscopy to characterize cooling–heating phase transitions in complete hypersaline microalgal culture media. The results provide new insight into the thermodynamics and kinetics of multicomponent brine systems and contribute to understanding the stability, storage, and cryobiological behavior of hypersaline cultivation media.

2. Materials and Methods

2.1. Composition and Rationale for Selection of Culture Media

The cooling–heating phase behavior of hypersaline culture media was investigated using two formulations commonly applied for the cultivation of *Dunaliella salina*: Artari (A) and Ramaraj (Rm) media. These media were selected because they represent two contrasting cultivation strategies—stress-induced metabolic activation and optimized biomass production—while differing substantially in ionic complexity and salinity. The detailed chemical compositions are summarized in Table 1.

Table 1. Chemical composition of Artari and Ramaraj culture media used in this study. Concentrations of micronutrients and macronutrients are given in $mg \cdot L^{-1}$ and $g \cdot L^{-1}$, respectively. For the Ramaraj medium, two NaCl concentrations (1.5 M and 4.0 M) were prepared to investigate the effect of salinity on phase behavior. Reported pH values correspond to the prepared media.

Chemicals	Artary	Ramaraj 1	Ramaraj 2
		Micronutrients (mg/L)	
H_3BO_3	–	9.28	9.28
$CoCl_2 \times 6H_2O$	–	0.05	0.05
$ZnCl_2$	–	0.11	0.11
$MnCl_2 \times 4H_2O$	–	1.98	1.98
Na_2MoO_4	–	0.49	0.49
$NaVO_3$	–	0.24	0.24
$CuCl_2 \times 6H_2O$	–	0.05	0.05

Table 1. *Cont.*

Chemicals	Artary	Ramaraj 1	Ramaraj 2
	Macronutrients (g/L)		
$MgSO_4 \times 7H_2O$	50.0	1.23	1.23
KCl	–	0.2	0.2
$CaCl_2 \times 2H_2O$	–	0.044	0.044
KNO_3	2.5	0.5	0.5
KH_2PO_4	0.2	0.014	0.014
$FeCl_3 \times 6H_2O$	–	0.0005	0.0005
Na_2EDTA	–	0.074	0.074
$NaHCO_3$	1.0	2.1	2.1
NaCl	116.0	87.7 (1.5 M)	233.76 (4 M)
pH	7	7.2	7.2

The Artari medium is a classical hypersaline formulation introduced in the 1960–1970s for the cultivation of *Dunaliella* and other halophiles. It is characterized by a relatively simplified ionic composition dominated by sodium chloride (116 $g \cdot L^{-1}$, approximately 2.0 M NaCl) and containing a limited set of macronutrients (primarily Mg^{2+}, K^+, nitrogen, phosphorus, and carbon sources). Notably, the formulation is intentionally depleted in trace microelements.

This reduced microelement composition induces controlled physiological stress in *D. salina*, promoting the accumulation of protective metabolites such as β-carotene, glycerol, and antioxidant compounds. Consequently, the Artari medium is widely used in studies of salt-induced metabolic adaptation and mimics stress conditions characteristic of natural hypersaline lakes.

The pH of the Artari medium was adjusted to 7.0 using dilute NaOH or HCl solutions and measured with a calibrated laboratory pH meter.

The Ramaraj medium, as described in previous studies [6], was developed to optimize the growth performance of *D. salina*. In contrast to Artari, this formulation contains a broader spectrum of inorganic components, including trace elements (B, Co, Zn, Mn, Mo, V, Cu) and modified salt ratios, particularly elevated $MgSO_4$ concentrations.

The Ramaraj medium has been reported to support faster cell division (approximately 1.5–3-fold higher growth rates), increased biomass accumulation, and improved adaptation across a salinity range of 0.5–2.5 M NaCl compared with simplified basal media. It is therefore suitable for controlled cultivation aimed at maximizing biomass production under hypersaline conditions.

To assess salinity-dependent phase behavior, the Ramaraj medium was prepared at two NaCl concentrations:

- 1.5 M NaCl (Ramaraj 1), corresponding to conditions favorable for rapid growth and biomass accumulation;
- 4.0 M NaCl (Ramaraj 2), corresponding to hyperosmotic stress conditions used for carotenoid induction.

These concentrations reflect standard experimental approaches in *Dunaliella* research, where moderate salinity supports growth optimization and elevated salinity promotes metabolic stress responses.

The pH of both Ramaraj variants was adjusted to 7.2 using dilute NaOH or HCl solutions.

Analytical-grade reagents (Merck KGaA, Darmstad, Germany) and ultrapure water (resistivity 18.2 MΩ·cm at 25 °C) obtained from a Milli-Q purification system (Millipore, Billerica, MA, USA) were used for the preparation of all media. Individual components were dissolved sequentially under continuous magnetic stirring until complete dissolution. Solutions were visually inspected to confirm the absence of undissolved solids prior to thermal analysis. Prepared media were used directly for differential scanning calorimetry (DSC) and cryomicroscopy without further modification.

2.2. Differential Scanning Calorimetry (DSC)

Thermal phase transitions of hypersaline culture media were investigated using a differential scanning calorimeter (Discovery X3, TA Instruments, New Castle, DE, USA) equipped with a refrigerated cooling system (RCS).

The instrument was calibrated for temperature and enthalpy according to the manufacturer's procedures using certified reference materials: indium and adamantane standards. The melting transition of deionized water was used to verify temperature accuracy in the subzero region. Heat capacity calibration was performed using a sapphire standard. Separate calibration files were applied for each heating rate.

Aliquots of 10–20 mg of culture medium were hermetically sealed in Tzero aluminum pans (TA Instruments, P/N: 901683.901) with Tzero hermetic lids (P/N: 901684.901) to prevent evaporation and compositional changes during thermal cycling. Empty sealed pans of identical type were used as a reference. The Tzero pan–lid configuration ensures optimal thermal contact and enables full utilization of the four-sensor architecture of the Discovery X3, thereby improving baseline stability and heat-flow accuracy.

Samples were cooled from room temperature to the target subzero temperature at controlled rates and subsequently heated at either 5 °C·min^{-1} or 10 °C·min^{-1}, depending on the experimental series. The use of two heating rates allowed assessment of kinetic effects on phase transitions and potential recrystallization phenomena during warming. All measurements were performed under a dry nitrogen purge (50 mL·min^{-1}).

Peak onset temperatures and enthalpy values were determined using TA Instruments analysis software. Enthalpy values were calculated by integrating peak areas relative to a linear baseline constructed between pre- and post-transition regions. For overlapping transitions, integration limits were defined using inflection points in the heat-flow curve.

2.3. Cryomicroscopy

Cooling–heating phase transitions in hypersaline culture media were investigated using an open-source hardware- and software-based cryomicroscopy platform previously developed, characterized, and validated for cryobiological research [23]. The system integrates a transmitted-light optical microscope with a custom-designed temperature-controlled cryochamber and an Arduino-based electronic control unit, enabling programmable thermal cycling and real-time visualization of phase transitions.

The cryomicroscopy setup consisted of a transmitted-light optical microscope (Carl Zeiss, Oberkochen, Germany) equipped with a custom-fabricated fluoropolymer cryochamber (internal volume approximately 10 mL) mounted on the microscope stage. Samples were placed on a sapphire crystal substrate (thickness 0.15 mm), which served as a highly thermally conductive support to ensure rapid and spatially uniform temperature equilibration.

Temperature control was implemented using an Arduino Uno Rev3 microcontroller (ATmega16U2 architecture, Chandler, AZ, USA) coupled to a resistance temperature detector (RTD; TEM-006-05, Dnipro, Ukraine) interfaced via a MAX31865 converter (Analog Devices, Wilmington, MA, USA). Independent temperature validation was performed using a K-type thermocouple connected through a MAX31855 amplifier (Analog Devices,

Wilmington, MA, USA), enabling cross-verification of thermal measurements. Cooling was achieved by controlled nitrogen vapor flow generated from liquid nitrogen in a Dewar vessel equipped with an electrically heated spiral. Image acquisition and video recording were performed using a digital USB microscope camera connected to a computer. A schematic representation of the experimental setup and electronic architecture is provided in the original validation study [23].

Temperature regulation was achieved by modulating nitrogen vapor flow via pulse-width control of the heating element using a custom Arduino control script. Unless otherwise specified, samples were cooled at a programmed rate of 1 °C·min^{-1}.

The RTD sensor was positioned in direct mechanical and thermal contact with the sapphire substrate to minimize thermal lag between measured and actual sample temperature. System accuracy was previously assessed by comparing measured melting temperatures of distilled water and saline reference solutions with theoretical values. Under the applied experimental conditions, temperature deviation did not exceed ±0.2 °C, which is sufficient to resolve melting-point depression, nucleation events, eutectic crystallization, and recrystallization phenomena.

The simultaneous use of two independent temperature sensors (RTD and thermocouple) enabled cross-validation of temperature readings and verification of thermal stability during cooling–warming cycles. Each complete cooling–warming cycle from +20 °C to −50 °C required approximately 0.5 L of liquid nitrogen.

Cell-free culture media (5 µL aliquots) were pipetted onto the sapphire substrate and gently covered with a cover glass, resulting in a confined sample layer approximately 65 µm thick. This geometry ensured adequate optical resolution while limiting vertical crystal growth. Samples were equilibrated at 20 °C for 3 min prior to cooling.

Due to geometric confinement between the sapphire substrate and cover glass, crystal growth in the vertical direction was restricted. Consequently, quantitative ice-size measurements were performed in the focal plane and reported as two-dimensional projected diameters.

Samples were cooled from +20 °C to −50 °C at 1 °C·min^{-1} using controlled nitrogen vapor flow. After a 1 min isothermal hold at −50 °C, active cooling was discontinued, and samples were allowed to passively rewarm to room temperature over approximately 20 min.

Phase transitions were continuously recorded using the digital camera attached to the microscope optical output. Video sequences were analyzed frame-by-frame to determine ice nucleation temperature (onset of first visible crystallization), final melting temperature (disappearance of the last ice crystal), presence or absence of salt eutectic crystallization (identified as dark intercrystalline regions), recrystallization during warming, formation of non-crystalline or amorphous phases, ice crystal morphology, and average projected ice crystal diameter at predefined temperatures. Representative frames and synchronized temperature data were extracted from recorded video sequences for quantitative analysis.

Each medium composition was examined in at least three independent experiments. Reported transition temperatures were extracted from thermal profiles synchronized with video timestamps. Observations were consistent across replicates, and no significant variation in qualitative phase behavior was observed between experiments.

2.4. Statistical Analysis

All statistical analyses were performed using R software (version 4.3.1). Data presented in tables are expressed as mean ± standard deviation (SD), with sample sizes indicated where applicable. No significant outliers were identified within replicate datasets.

3. Results

3.1. DSC Analysis of Phase Behavior in Saline Culture Media During Cooling–Heating Cycles

Differential scanning calorimetry revealed pronounced differences in the phase-transition behavior of saline culture media depending on medium composition, sodium chloride concentration, and the applied cooling–heating conditions. Representative DSC thermograms recorded using the Discovery X3 calorimeter during cooling and subsequent heating are shown in Figures 1–3, while quantitative parameters of the detected transitions are summarized in Tables 2–4. The thermal events labeled C1–C3 and M1–M3 in Figures 1–3 correspond to the crystallization and melting transitions listed in Tables 2–4.

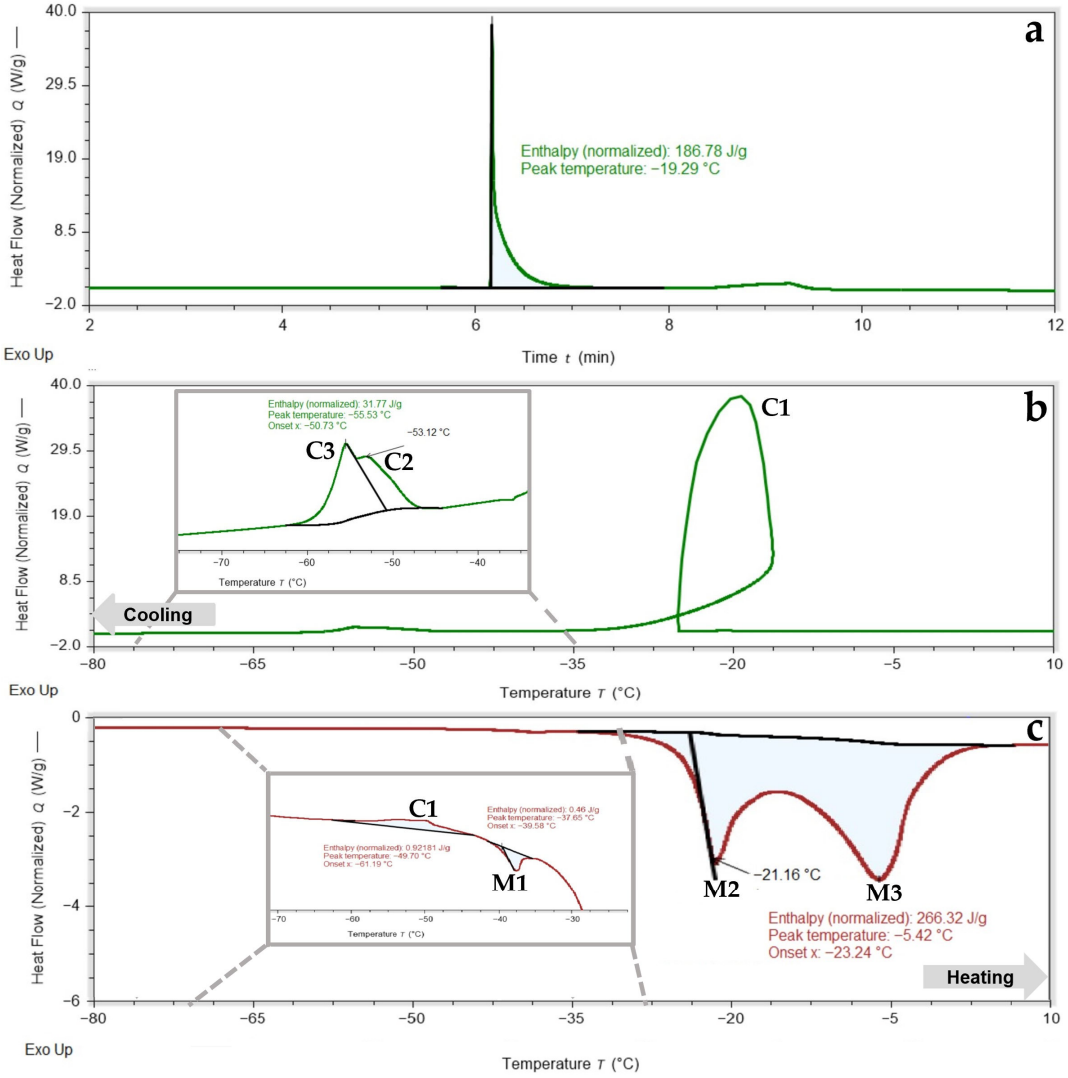


Figure 1. Differential scanning calorimetry (DSC) thermograms of the Ramaraj 1 culture medium containing 1.5 M NaCl, recorded using a Discovery X3 DSC during cooling and heating at 10 °C·min^{-1}. (**a**) Heat-flow signal plotted as a function of time during cooling, showing an exothermic peak corresponding to ice crystallization. (**b**) Heat-flow signal as a function of temperature during cooling, illustrating crystallization events labeled C1–C3 (C = crystallization), corresponding to the thermal transitions summarized in Table 2; the inset shows a magnified region highlighting secondary crystallization events at lower temperatures. (**c**) Heat-flow signal during subsequent heating, showing an exothermic event labeled C1 (C = crystallization) and endothermic transitions labeled M1–M3 (M = melting), corresponding to the events reported in Table 2; the inset highlights low-temperature thermal features preceding the main melting transition. Cooling curves are shown in green and heating curves in red, while the black line represents the baseline used for peak integration. Exothermic heat flow is plotted upward.

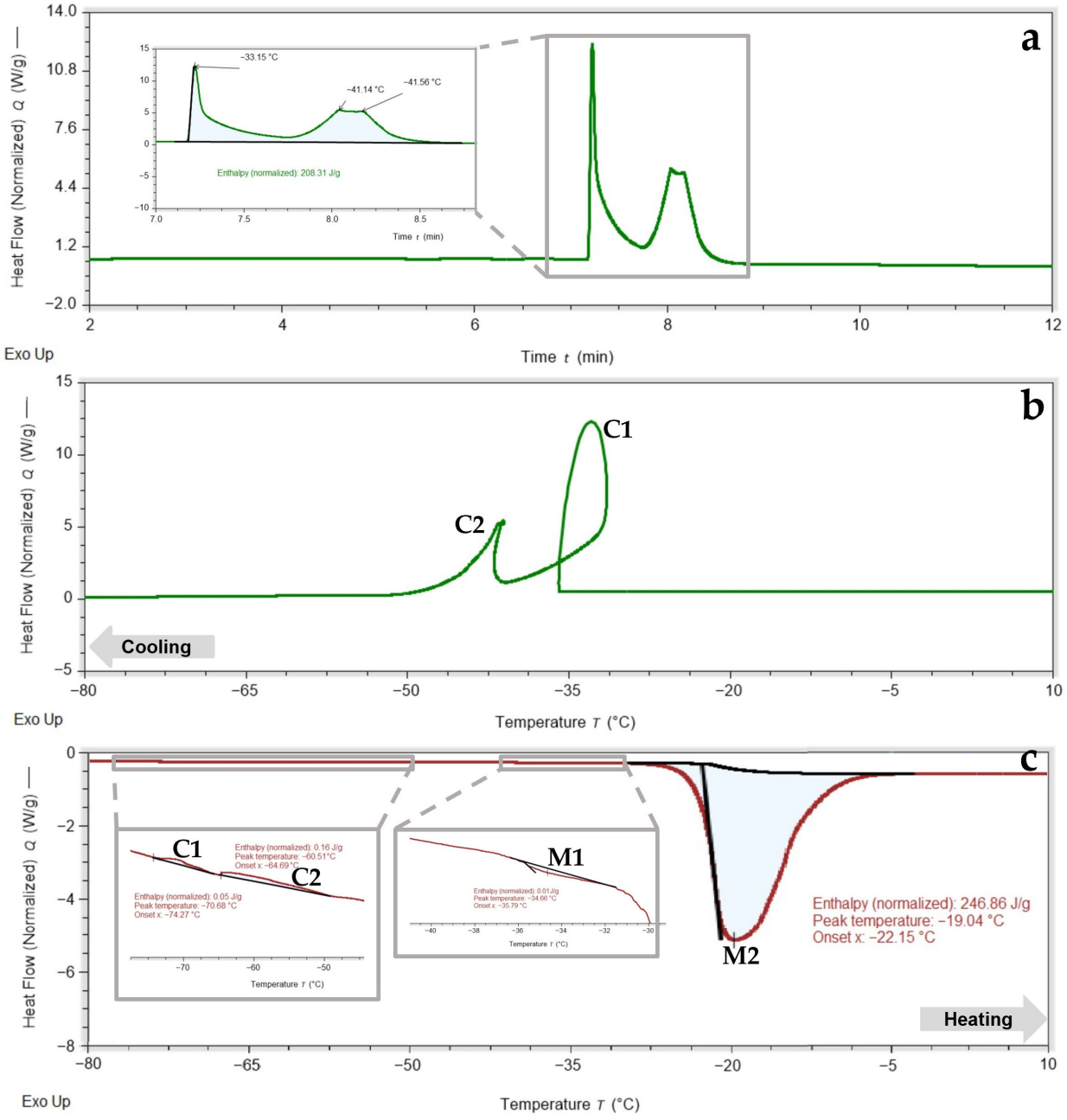


Figure 2. Differential scanning calorimetry (DSC) thermograms of the Ramaraj 2 culture medium containing 4.0 M NaCl, recorded using a Discovery X3 DSC during cooling, and heating at 10 °C·min^{-1}. (**a**) Heat-flow signal plotted as a function of time during cooling, showing exothermic crystallization events (inset highlights the complex shape of the crystallization peak). (**b**) Heat-flow signal as a function of temperature during cooling, illustrating crystallization events labeled C1 and C2 (C = crystallization), corresponding to the transitions summarized in Table 3 and demonstrating delayed and broadened crystallization typical of highly saline media. (**c**) Heat-flow signal during subsequent heating, showing exothermic events labeled C1 and C2 (C = crystallization) and endothermic transitions labeled M1 and M2 (M = melting), corresponding to the thermal events reported in Table 3; the insets highlight low-temperature features preceding the main melting peak. Cooling curves are shown in green and heating curves in red, while the black line represents the baseline used for peak integration. Exothermic heat flow is plotted upward.

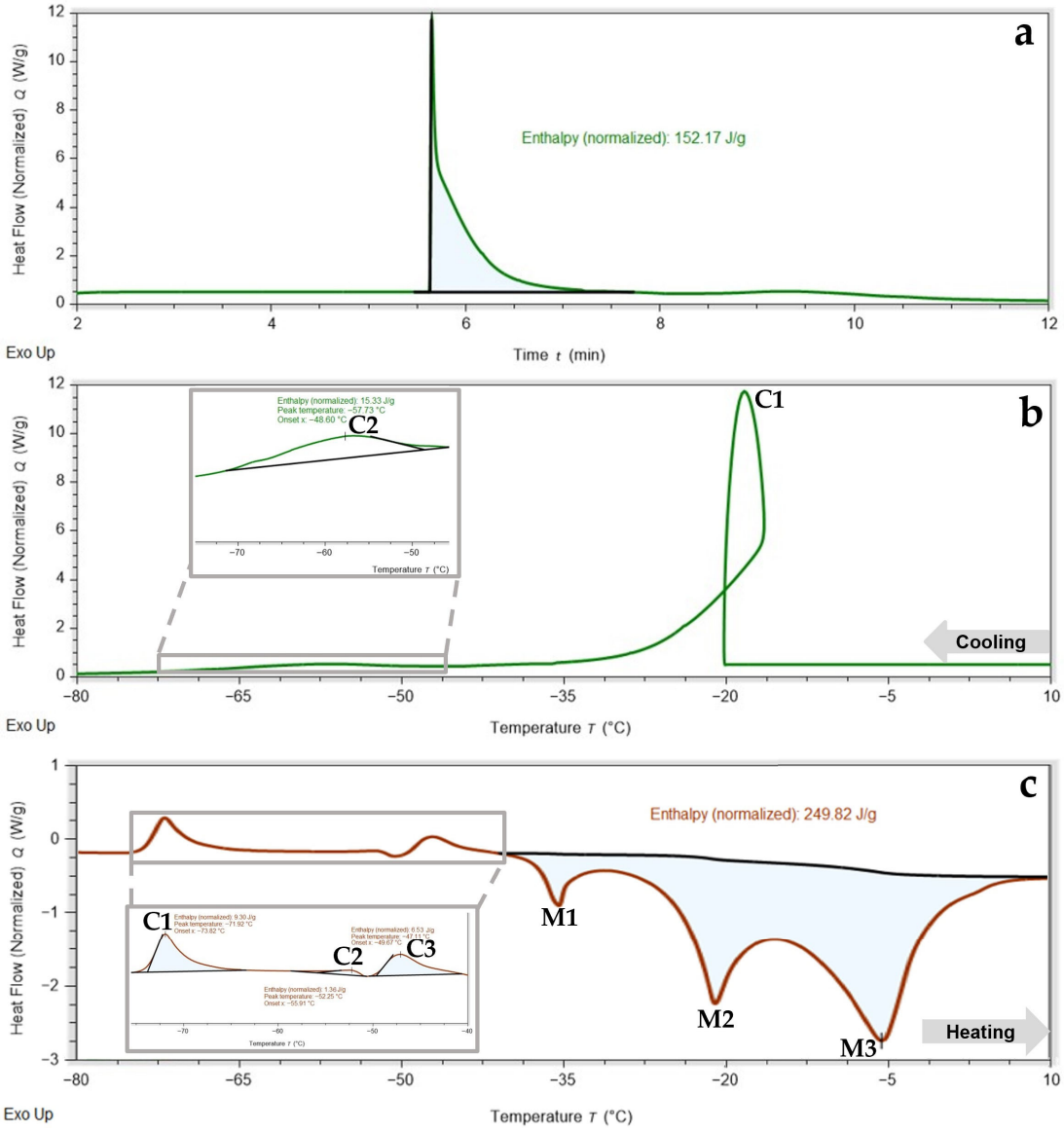


Figure 3. Differential scanning calorimetry (DSC) thermograms of the Artari culture medium containing 2.0 M NaCl, recorded using a Discovery X3 DSC during cooling and heating at 10 °C·min^{-1}. (**a**) Heat-flow signal plotted as a function of time during cooling, showing a pronounced exothermic peak corresponding to ice crystallization. (**b**) Heat-flow signal as a function of temperature during cooling, illustrating crystallization events labeled C1 and C2 (C = crystallization), corresponding to the transitions summarized in Table 4; the inset highlights the low-temperature crystallization event. (**c**) Heat-flow signal during subsequent heating, showing exothermic events labeled C1–C3 (C = crystallization) and endothermic transitions labeled M1–M3 (M = melting), corresponding to the events reported in Table 4; the insets highlight additional low-temperature thermal features observed prior to the main melting transition. Cooling curves are shown in green and heating curves in red, while the black line represents the baseline used for peak integration. Exothermic heat flow is plotted upward.

During cooling at 10 °C·min^{-1}, the Ramaraj 1 medium containing 1.5 M NaCl exhibited a dominant exothermic crystallization event (Crystallization 1) with an onset temperature near −25 °C (Figure 1a,b; Table 2). This transition was associated with a large enthalpy release, indicating crystallization of the major fraction of free water. At lower temperatures, additional weaker exothermic events (Crystallization 2 and 3) were detected in some cooling protocols, suggesting the presence of secondary crystallization processes occurring in increasingly concentrated residual solutions.

Table 2. Temperatures and enthalpies of phase transitions in Ramaraj 1 culture medium containing 1.5 M NaCl were determined by differential scanning calorimetry during cooling–heating cycles at different temperature rates. Crystallization and melting events are listed in the order of their appearance during cooling or heating. Data is presented as mean ± SD.

Phase Transition	Parameter	Cooling (°C/min)/Heating (°C/min) 10/10 (1)		20/5 (2)	
		Cooling Stage	Heating Stage	Cooling Stage	Heating Stage
Crystallization 1	T, °C	−25.2 ± 0.01	−60.7 ± 1.0	−20.1 ± 0.1	−61.5 ± 1.0
	Enthalpy, J/g	183 ± 3	0.877 ± 0.059	183 ± 6	0.011 ± 0.001
Crystallization 2	T, °C	−48.3 ± 0.5	–	−45.0 ± 0.1	0
	Enthalpy, J/g	6.92 ± 0.17	–	21.4 ± 0.3	0
Crystallization 3	T, °C	−55.4 ± 0.1	–	−57.0 ± 0.2	0
	Enthalpy, J/g	24.6 ± 0.6	–	7.20 ± 0.28	0
Melting 1	T, °C	–	−39.6 ± 0.1	–	−38.6 ± 0.5
	Enthalpy, J/g	–	0.47 ± 0.03	–	0.03 ± 0.01
Melting 2	T, °C	–	−23.5 ± 0.4	–	−22.9 ± 0.1
	Enthalpy, J/g	–	114 ± 3	–	113 ± 1
Melting 3	T, °C	–	−11.4 ± 0.1	–	11.8 ± 0.1
	Enthalpy, J/g	–	151 ± 4	–	155 ± 1

Table 3. Temperatures and enthalpies of phase transitions in Ramaraj 2 culture medium containing 4.0 M NaCl were determined by differential scanning calorimetry during cooling–heating cycles at different temperature rates. Crystallization and melting events are listed in the order of their appearance during cooling or heating. Data is presented as mean ± SD.

Phase Transition	Parameter	Cooling/Warming Rate, °C/min 10/10		20/5	
		Cooling Stage	Heating Stage	Cooling Stage	Heating Stage
Crystallization 1	T, °C	−35.9 ± 0.1	−74.6 ± 0.3	−32.9 ± 0.1	−65.5 ± 0.2
	Enthalpy, J/g	96.6 ± 0.4	0.05 ± 0.01	96.5 ± 0.7	0.126 ± 0.009
Crystallization 2	T, °C	−42.1 ± 0.1	−64.7 ± 0.1	−42.8 ± 0.4	−53.9 ± 0.3
	Enthalpy, J/g	112 ± 1	0.155 ± 0.009	104 ± 1	0.016 ± 0.001
Melting 1	T, °C	–	−35.8 ± 0.1	–	−36.8 ± 0.1
	Enthalpy, J/g	–	0.012 ± 0.003	–	0.030 ± 0.001
Melting 2	T, °C	–	−22.1 ± 0.1	–	−22.2 ± 0.1
	Enthalpy, J/g	–	247 ± 1	–	243 ± 1

Table 4. Temperatures and enthalpies of phase transitions in Artari culture medium (2.0 M NaCl) were determined by differential scanning calorimetry during cooling–heating cycles at different temperature rates. Crystallization and melting events are listed in the order of their appearance during cooling or heating. Data are presented as mean ± SD.

Phase Transition	Parameter	Cooling/Warming Rate, °C/min 10/10		20/5	
		Cooling Stage	Heating Stage	Cooling Stage	Heating Stage
Crystallization 1	T, °C	−20.4 ± 0.3	−73.8 ± 0.01	−25.0 ± 0.1	−64.1 ± 0.1
	Enthalpy, J/g	152 ± 2	9.40 ± 0.09	156 ± 2	13.9 ± 1.2
Crystallization 2	T, °C	−48.7 ± 0.2	−56.0 ± 0.3	–	−55.5 ± 0.1
	Enthalpy, J/g	15.9 ± 0.5	1.41 ± 0.17	–	0.75 ± 0.03
Crystallization 3	T, °C	–	−49.7 ± 0.1	–	−52.2 ± 0.1
	Enthalpy, J/g	–	6.81 ± 0.32	–	5.14 ± 0.24
Melting 1	T, °C	–	−37.8 ± 0.2	–	−37.7 ± 0.1
	Enthalpy, J/g	–	31.5 ± 0.1	–	10.5 ± 0.2

Table 4. *Cont.*

Phase Transition	Parameter	Cooling/Warming Rate, °C/min 10/10		20/5	
		Cooling Stage	Heating Stage	Cooling Stage	Heating Stage
Melting 2	T, °C	–	−23.9 ± 0.1	–	−24.6 ± 0.4
	Enthalpy, J/g	–	101 ± 3	–	77.2 ± 1.0
Melting 3	T, °C	–	−14.2 ± 0.6	–	−16.3 ± 0.9
	Enthalpy, J/g	–	143 ± 3	–	123 ± 1

Upon subsequent heating, multiple endothermic transitions were observed (Figure 1c), corresponding to the melting of ice fractions formed during cooling.

The principal melting peak (Melting 2), centered near −23 °C, accounted for the largest portion of the total melting enthalpy. Smaller endothermic events at lower temperatures were also detected, likely reflecting the melting of ice formed in solute-enriched microenvironments.

Modification of the thermal protocol—specifically, increasing the cooling rate to 20 °C·min^{-1} and reducing the heating rate to 5 °C·min^{-1}—resulted in shifts in crystallization and melting temperatures and redistribution of enthalpy among individual transitions (Table 2), indicating kinetic sensitivity of phase formation and subsequent melting behavior.

Increasing salinity to 4.0 M NaCl substantially altered the DSC response (Figure 2). During cooling, crystallization shifted to lower temperatures and occurred over a broader temperature interval compared with the 1.5 M medium. The enthalpy associated with individual crystallization events was reduced, indicating that a smaller fraction of water participated in crystallization under these conditions.

During heating, the melting behavior of the 4.0 M medium was dominated by a single major endothermic transition near −22 °C, accompanied by low-enthalpy events at lower temperatures (Table 3). The overall melting enthalpy was lower than that observed for the Ramaraj 1 medium, reflecting enhanced suppression of ice formation at higher salinity. Changes in cooling–heating rates primarily affected the relative contribution of minor thermal events but did not eliminate the main melting transition.

The Artari medium exhibited a distinct DSC profile compared with the Ramaraj formulations. During cooling, a pronounced crystallization event was detected at approximately −20 °C (Figure 3a,b), accompanied by a relatively high enthalpy release (Table 4). Additional low-temperature crystallization events were occasionally observed, depending on the cooling protocol.

Upon heating, the Artari medium displayed multiple melting transitions extending from approximately −38 °C to −1 °C (Figure 3c). The cumulative melting enthalpy was higher than that observed for the Ramaraj media, indicating a larger fraction of crystallized water. No clear glass-transition-related baseline shift was detected within the accessible temperature range of the Discovery X3 DSC under the applied experimental conditions.

In all investigated media, crystallization events were occasionally observed not only during cooling but also during subsequent heating. Such behavior indicates that complete crystallization was not achieved during cooling and that a fraction of the solution remained in a non-crystalline, kinetically constrained state at low temperatures. Upon warming, this fraction underwent delayed crystallization before melting.

This behavior is characteristic of systems in which increasing solute concentration during freezing leads to kinetic arrest of part of the unfrozen fraction, potentially resulting in formation of an amorphous or highly viscous phase that remains undetected within the accessible temperature range.

Taken together, these results indicate that salinity and thermal history strongly influence the balance between crystalline and non-crystalline fractions in hypersaline culture media.

3.2. Cryomicroscopy Analysis of Phase Behavior in Saline Culture Media

Cryomicroscopic observations of saline culture media during controlled cooling–heating cycles revealed pronounced differences in ice morphology and its evolution depending on medium composition and sodium chloride concentration. Representative micrographs for the Ramaraj and Artari media are shown in Figures 4–6.

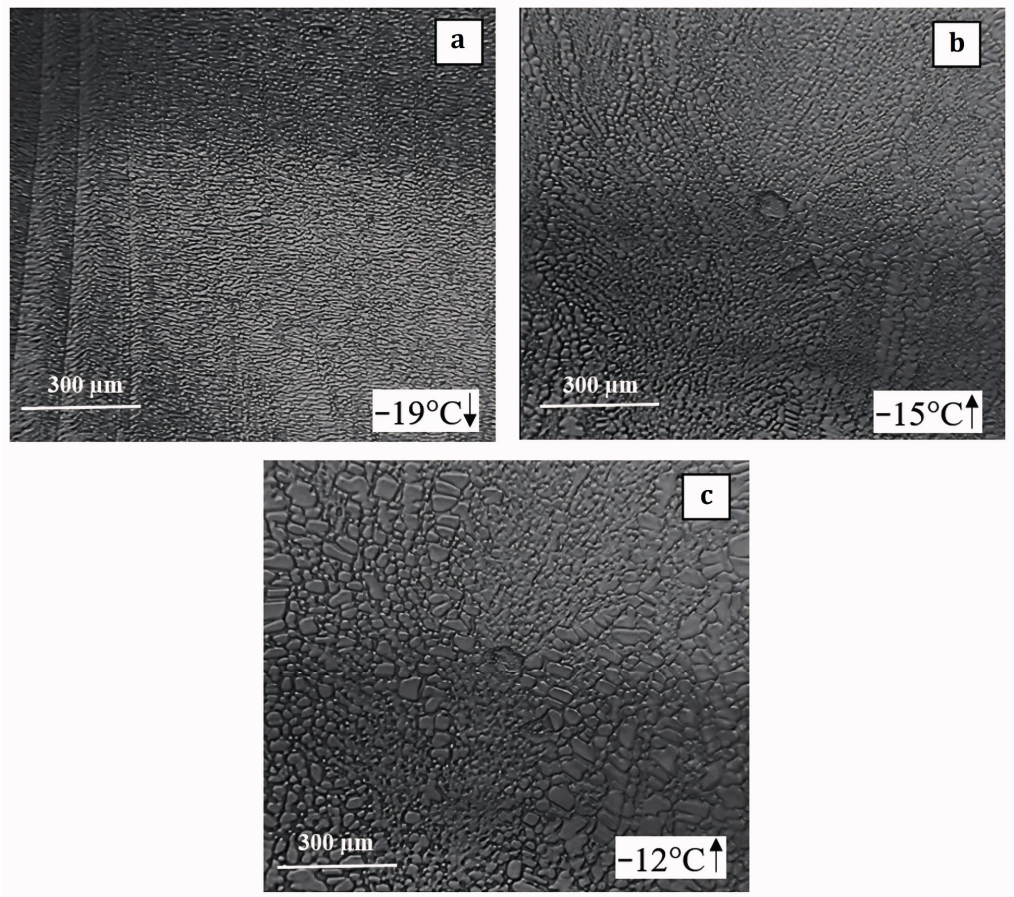


Figure 4. Cryomicroscopy images illustrating the cooling–heating phase transitions in Ramaraj 1 culture medium containing 1.5 M NaCl. (**a**) Formation of fine-crystalline ice structure during the cooling stage at −19 °C. (**b**,**c**) Progressive increase in ice crystal size during subsequent heating at −15 °C and −12 °C, respectively, indicating recrystallization processes. Arrows indicate the direction of temperature change: ↓ cooling; ↑ heating. Scale bar: 300 µm.

During cooling of the Ramaraj 1 medium containing 1.5 M NaCl, ice nucleation resulted in the formation of a fine-crystalline structure distributed uniformly throughout the sample (Figure 4a). The ice crystals were small and densely packed, consistent with rapid ice nucleation under moderate cooling conditions.

Upon subsequent heating, a gradual increase in crystal size was observed (Figure 4b,c). This process was characterized by coarsening of the initial fine-crystalline ice network, leading to the formation of larger, more clearly defined crystals as the temperature increased from −15 °C to −12 °C. The observed structural changes indicate active recrystallization during the heating stage.

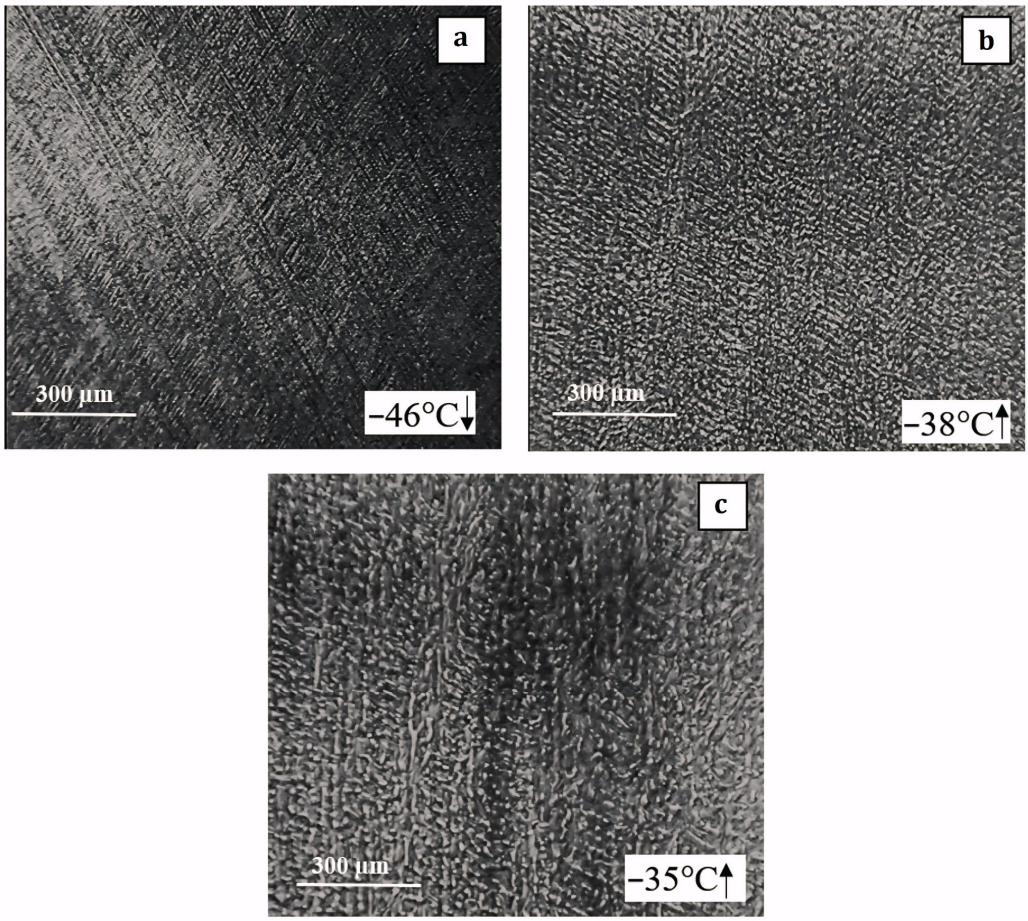


Figure 5. Cryomicroscopy images illustrating the cooling–heating phase transitions in Ramaraj 2 culture medium containing 4.0 M NaCl. (**a**) Formation of a highly fine-grained ice structure during the cooling stage at −46 °C. (**b**,**c**) Limited increase in ice crystal size during subsequent heating at −38 °C and −35 °C, respectively, indicating suppressed recrystallization in a highly saline medium. Arrows indicate the direction of temperature change: ↓ cooling; ↑ heating. Scale bar: 300 µm.

In contrast, the Ramaraj 2 medium with 4.0 M NaCl exhibited markedly different ice morphology during cooling. At −46 °C, the sample displayed a highly fine-grained ice structure with limited crystal growth (Figure 5a). The increased salinity appeared to restrict ice crystal growth and promote a more homogeneous microstructure.

During heating, only limited changes in crystal size and morphology were detected between −38 °C and −35 °C (Figure 5b,c). Compared with the 1.5 M medium, crystal coarsening was less pronounced, and the fine-grained structure persisted over a broader temperature range, indicating reduced recrystallization activity at elevated salinity.

The Artari medium exhibited a distinct pattern of ice formation and evolution. During cooling, a fine-crystalline ice structure formed at approximately −26 °C (Figure 6a). Further cooling to −36 °C resulted in the development of a coarse polycrystalline morphology with clearly visible crystal boundaries (Figure 6b).

Upon heating, partial restructuring and coarsening of ice crystals were observed at −18 °C (Figure 6c). The resulting microstructure consisted of larger, irregularly shaped crystals, indicating ongoing recrystallization during warming. Compared with the Ramaraj 2 medium at 4.0 M NaCl, the Artari medium showed more pronounced morphological changes during heating.

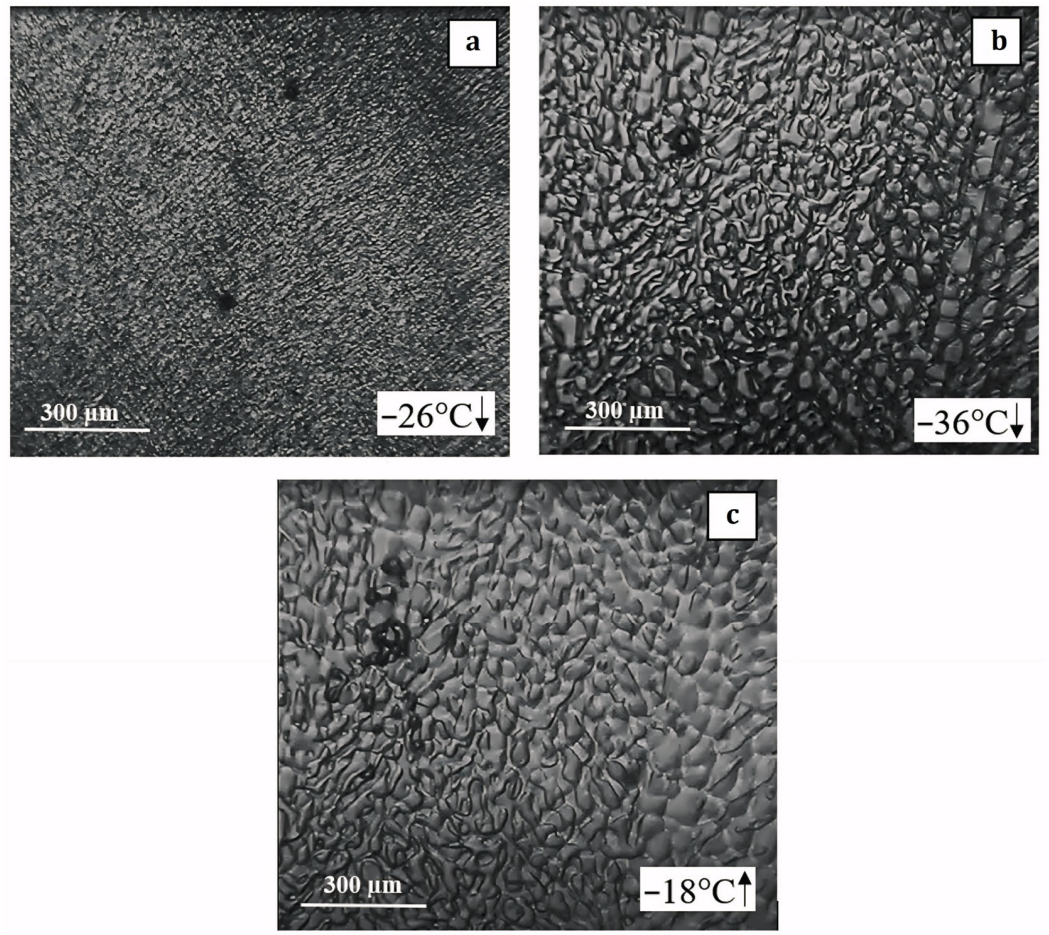


Figure 6. Cryomicroscopy images illustrating the cooling–heating phase transitions in Artari culture medium containing 2.0 M NaCl. (**a**) Formation of a fine-crystalline ice structure during the cooling stage at −26 °C. (**b**) Development of a coarse polycrystalline ice morphology during further cooling at −36 °C. (**c**) Partial coarsening and restructuring of ice crystals during subsequent heating at −18 °C. Arrows indicate the direction of temperature change: ↓ cooling; ↑ heating. Scale bar: 300 µm.

4. Discussion

The present study provides a physicochemical characterization of hypersaline culture media formulated for *D. salina*, combining differential scanning calorimetry and cryomicroscopy to elucidate how salinity, medium composition, and thermal history govern phase behavior during cooling–heating cycles. The results demonstrate that these multicomponent hypersaline systems exhibit complex crystallization pathways, pronounced kinetic effects, and behavior consistent with partial vitrification, extending beyond the behavior expected for simple NaCl–water solutions.

The observed phase-transition behavior can be interpreted in the context of the well-characterized NaCl–water phase diagram and freezing behavior of saline brines. In binary NaCl–water systems, ice crystallization typically occurs near the liquidus temperature, followed by progressive solute exclusion into the remaining liquid phase during freezing. As temperature decreases, the residual solution becomes increasingly concentrated until the eutectic composition is reached. The equilibrium eutectic temperature of the NaCl–water system (approximately −21.2 °C) corresponds to the simultaneous crystallization of ice and hydrohalite ($NaCl{\cdot}2H_2O$). As a result, freezing produces a heterogeneous microstructure consisting of ice crystals separated by highly concentrated brine channels. Numerous experimental and theoretical studies have demonstrated that increasing salinity

depresses freezing temperatures, modifies nucleation kinetics, and promotes the persistence of unfrozen brine fractions at low temperatures [4,12,13].

DSC analysis revealed a systematic suppression of ice crystallization with increasing NaCl concentration, manifested as a shift in crystallization to lower temperatures, broadening of crystallization peaks, and a reduction in total melting enthalpy. These effects were most pronounced in the Ramaraj 2 medium at 4.0 M NaCl. Such behavior is consistent with classical colligative effects, including freezing-point depression and reduced water activity, as well as with kinetic inhibition of ice nucleation and growth in concentrated electrolyte solutions [12,13,15]. Importantly, the decrease in melting enthalpy directly reflects a reduction in the fraction of crystallized water, indicating that a larger proportion of water remains in the unfrozen phase as salinity increases.

However, the culture media investigated here differ fundamentally from binary NaCl–water systems because they contain multiple inorganic salts, buffering agents, and trace components. In multicomponent electrolyte systems, phase equilibria become considerably more complex due to ion-specific interactions, competing eutectic systems, and differences in solubility among individual salts. These factors can modify crystallization temperatures, alter the composition of freeze-concentrated liquids, and influence the kinetics of ice nucleation and growth. Similar behavior has been reported for confined or multicomponent salt solutions in which crystallization occurs through multiple overlapping processes [15,24].

Cryomicroscopy observations strongly supported these calorimetric results. Media with elevated salinity formed fine-grained ice structures during cooling, which persisted during heating with only limited crystal coarsening. In contrast, media with lower effective salinity exhibited pronounced recrystallization during warming. Recrystallization is a key process governing structural evolution in frozen aqueous systems and depends strongly on solute concentration and molecular mobility within the residual liquid phase [16,17,20]. The suppression of recrystallization observed at high salinity, therefore, reflects reduced molecular mobility in highly concentrated interstitial phases.

A notable feature observed across all investigated media was the occurrence of crystallization events not only during cooling but also during subsequent heating. Crystallization-on-heating is characteristic of systems in which complete crystallization is avoided during cooling and part of the solution becomes kinetically trapped in a non-equilibrium state [25–29]. Upon warming, this fraction undergoes delayed crystallization prior to melting. Such behavior is commonly associated with partially vitrified or highly viscous freeze-concentrated phases formed during rapid solute enrichment during freezing.

Importantly, differences between Artari and Ramaraj media at comparable salinity levels indicate that phase behavior is governed not only by NaCl concentration but also by overall medium composition. The Artari medium consistently exhibited higher crystallization and melting enthalpies and more pronounced recrystallization during heating, suggesting a larger fraction of crystallizable water. In contrast, the more complex ionic composition of the Ramaraj medium, particularly at high salinity, appears to enhance kinetic arrest of the freeze-concentrated liquid phase and enhance persistence of non-crystalline fractions. These observations highlight the importance of multicomponent ionic interactions in determining phase-transition pathways in hypersaline solutions [30,31].

Previous studies have shown that multicomponent electrolyte systems can exhibit glass-transition temperatures, crystallization kinetics, and devitrification behavior markedly different from those of binary salt–water solutions [27,30–32]. The present results extend this understanding by demonstrating that complete hypersaline culture media behave as complex physicochemical systems in which phase transitions emerge from the combined effects of ionic strength, ion-specific interactions, and multicomponent solute coupling.

From a broader environmental perspective, the observed phase behavior may contribute to the resilience of halotolerant microorganisms such as *Dunaliella salina* in hypersaline ecosystems subject to temperature fluctuations. Suppression of ice crystallization, reduced recrystallization during warming, and the formation of partially vitrified interstitial phases can collectively mitigate mechanical stress, osmotic imbalance, and structural damage associated with freeze–thaw cycles [16,17,19,21]. These physicochemical characteristics may therefore contribute to the stability of hypersaline ecosystems experiencing seasonal or episodic cooling.

Such behavior is also relevant for understanding the stability of concentrated cryobrines in natural environments. Multicomponent saline solutions with depressed freezing points have been proposed as analogs of extraterrestrial cryobrines in planetary science, where highly concentrated salt solutions may persist in liquid or glassy states at subzero temperatures [22]. The complex freezing behavior observed in the present study, therefore, provides additional insight into the thermodynamic and kinetic processes governing the stability of concentrated brine systems under low-temperature conditions.

Although the present study did not directly assess cell survival, the identified physicochemical characteristics provide a mechanistic framework linking medium composition to extracellular stress conditions experienced by halophilic microorganisms. Similar relationships between extracellular phase behavior and biological outcomes have been demonstrated in cryobiological systems, where non-crystalline phases can stabilize cellular microenvironments during thermal cycling and reduce freeze-induced damage [20,25].

A limitation of the present work is the inability to directly quantify glass-transition phenomena at very low temperatures. Future studies employing DSC systems capable of controlled cooling and heating below −150 °C would allow direct determination of glass-transition temperatures and heat capacity changes. Complementary techniques such as dielectric spectroscopy or thermomechanical analysis could further clarify the nature and stability of the non-crystalline phases inferred from the present observations.

Extending the present approach to cell-containing systems would allow direct correlation between extracellular phase behavior and biological responses, providing deeper insight into the cryobiophysical mechanisms underlying halotolerance and thermal resilience in hypersaline microorganisms.

5. Conclusions

This study provides a systematic physicochemical characterization of the phase behavior of hypersaline culture media used for cultivation of *Dunaliella salina* during cooling–heating cycles, combining differential scanning calorimetry and cryomicroscopy. The results demonstrate that salinity, medium composition, and thermal history strongly influence ice crystallization, recrystallization during warming, and the formation of non-crystalline phases in these multicomponent aqueous systems.

Increasing sodium chloride concentration markedly suppressed ice crystallization, shifted crystallization events to lower temperatures, and reduced the fraction of crystallized water, with the strongest effects observed in the Ramaraj medium containing 4.0 M NaCl. Cryomicroscopy confirmed that elevated salinity promotes the formation of fine-grained ice structures and significantly reduces recrystallization during heating, indicating increased kinetic stabilization of the frozen microstructure.

The occurrence of crystallization during heating across all investigated media indicates that complete crystallization was not achieved during cooling and that a portion of the solution remained kinetically trapped in a non-crystalline state. This behavior is consistent with partial vitrification of the freeze-concentrated phase in highly saline media.

Comparison with classical NaCl–water systems further demonstrates that hypersaline algal culture media cannot be described as simple binary salt solutions. Instead, their phase behavior reflects the complex interplay of ionic strength, multicomponent composition, and kinetic effects associated with freeze concentration.

Overall, the combined calorimetric and microscopic approach used in this study provides new insight into the thermodynamic and kinetic processes governing freezing in multicomponent hypersaline media. These findings contribute to a better understanding of the stability of hypersaline environments under temperature fluctuations and provide a physicochemical basis for optimizing saline culture media used in algal biotechnology, cryobiology, and related applications.

Author Contributions: Conceptualization, O.B. and N.C.; methodology, O.B. and N.C.; validation, O.B., N.C., N.S. and V.H.; formal analysis O.B. and V.H.; investigation, O.B., N.C. and N.S.; resources, N.S.; data curation, O.B.; writing—original draft preparation, O.B. and N.C.; writing—review and editing, N.S., V.H. and A.S.; visualization, V.H., N.C. and O.B.; supervision, N.S. All authors have read and agreed to the published version of the manuscript.

Funding: This research was funded by the Ministry of Agriculture of the Czech Republic, the Institutional project number MZE-RO0425 and by National Academy of Sciences of Ukraine, project number 0121U108990.

Data Availability Statement: The original contributions presented in this study are included in the article. Further inquiries can be directed to the corresponding authors.

Conflicts of Interest: The authors declare no conflicts of interest.

References

1. Martínez, G.; Pire, C.; Martínez-Espinosa, R. Hypersaline environments as natural sources of microbes with potential applications in biotechnology: The case of solar evaporation systems to produce salt in Alicante County (Spain). *Curr. Res. Microb. Sci.* **2022**, *3*, 100136. [CrossRef]
2. Oren, A. Halophilic microbial communities and their environments. *Curr. Opin. Biotechnol.* **2015**, *33*, 119–124. [CrossRef] [PubMed]
3. Hosseini Tafreshi, A.; Shariati, M. *Dunaliella* biotechnology: Methods and applications. *J. Appl. Microbiol.* **2009**, *107*, 14–35. [CrossRef] [PubMed]
4. Chen, H.; Jiang, J. Osmotic responses of *Dunaliella* to the changes of salinity. *J. Cell. Physiol.* **2009**, *219*, 251–258. [CrossRef]
5. Barbosa, M.; Inácio, L.; Afonso, C.; Maranhão, P. The microalga *Dunaliella* and its applications: A review. *Appl. Phycol.* **2023**, *4*, 99–120. [CrossRef]
6. Chernobai, N.A.; Kadnikova, N.G.; Vozovyk, K.D.; Rozanov, L.F.; Kovalenko, I.F. Effects of salt stress and cooling regimes on the pigment composition of *Dunaliella salina* cells. *Biophys. Bull.* **2023**, *49*, 34–42. [CrossRef]
7. Chernobai, N.A.; Kadnikova, N.G.; Vozovyk, K.D.; Rozanov, L.F.; Kovalenko, I.F.; Kot, Y.G. Temperature-salt stress increases yield of valuable metabolites and shelf life of microalgae. *Biophys. Bull.* **2022**, *48*, 7–17. [CrossRef]
8. Pourkarimi, S.; Hallajisani, A.; Alizadehdakhel, A.; Nouralishahi, A.; Golzary, A. Factors affecting production of beta-carotene from *Dunaliella salina* microalgae. *Biocatal. Agric. Biotechnol.* **2020**, *29*, 101771. [CrossRef]
9. Schlipalius, L. The extensive commercial cultivation of *Dunaliella salina*. *Bioresour. Technol.* **1991**, *38*, 241–243. [CrossRef]
10. Colusse, G.; Mendes, C.; Duarte, M.; Carvalho, J.; Noseda, M. Effects of different culture media on physiological features and laboratory scale production cost of *Dunaliella salina*. *Biotechnol. Rep.* **2020**, *27*, e00508. [CrossRef]
11. Menzyanova, N.; Goltvyansky, A.; Kuznetsova, Y.; Sysenko, E. Season variability of iron effects on periodic culture of microalgae *Dunaliella viridis* Teod. *Front. Biol. China* **2009**, *4*, 328–336. [CrossRef]
12. Haghighi, H.; Chapoy, A.; Tohidi, B. Freezing Point Depression of Electrolyte Solutions: Experimental Measurements and Modeling Using the Cubic-Plus-Association Equation of State. *Ind. Eng. Chem. Res.* **2008**, *47*, 3983–3989. [CrossRef]
13. Koop, T.; Luo, B.; Tsias, A.; Peter, T. Water activity as the determinant for homogeneous ice nucleation in aqueous solutions. *Nature* **2000**, *406*, 611–614. [CrossRef]
14. Jiang, H.; Debenedetti, P.; Panagiotopoulos, A. Nucleation in aqueous NaCl solutions shifts from 1-step to 2-step mechanism on crossing the spinodal. *J. Chem. Phys.* **2019**, *150*, 124502. [CrossRef] [PubMed]

15. Koniorczyk, M.; Bednarska, D. Kinetics of water freezing from inorganic salt solution confined in mesopores. *Thermochim. Acta* **2019**, *682*, 178434. [CrossRef]
16. van Westen, T.; Groot, R. Predicting the Kinetics of Ice Recrystallization in Aqueous Sugar Solutions. *Cryst. Growth Des.* **2018**, *18*, 2405–2416. [CrossRef]
17. Zhu, Z.; Zhou, Q.; Sun, D. Measuring and controlling ice crystallization in frozen foods: A review of recent developments. *Trends Food Sci. Technol.* **2019**, *90*, 13–25. [CrossRef]
18. Wolfe, J.; Bryant, G. Cellular cryobiology: Thermodynamic and mechanical effects. *Int. J. Refrig.* **2001**, *24*, 438–450. [CrossRef]
19. Mazur, P. Freezing of living cells: Mechanisms and implications. *Am. J. Physiol. Cell Physiol.* **1984**, *247*, C125–C142. [CrossRef]
20. Murray, K.; Gibson, M. Chemical approaches to cryopreservation. *Nat. Rev. Chem.* **2022**, *6*, 579–593. [CrossRef] [PubMed]
21. Chang, T.; Zhao, G. Ice Inhibition for Cryopreservation: Materials, Strategies, and Challenges. *Adv. Sci.* **2021**, *8*, 2002425. [CrossRef]
22. Toner, J.; Catling, D.; Light, B. The formation of supercooled brines, viscous liquids, and low-temperature perchlorate glasses in aqueous solutions relevant to Mars. *Icarus* **2014**, *233*, 36–47. [CrossRef]
23. Pakhomov, O.; Shevchenko, N.; Chernobai, N.; Prokopiuk, V.; Yershov, S.; Bozhok, G. Open-source hardware- and software-based cryomicroscopy system for investigation of phase transitions in cryobiological research. *J. Microsc.* **2023**, *293*, 71–85. [CrossRef]
24. Macfarlane, D. Devitrification in glass-forming aqueous solutions. *Cryobiology* **1986**, *23*, 230–244. [CrossRef]
25. Fahy, G.; MacFarlane, D.; Angell, C.; Meryman, H. Vitrification as an approach to cryopreservation. *Cryobiology* **1984**, *21*, 407–426. [CrossRef]
26. Imrichová, K.; Veselý, L.; Gasser, T.; Loerting, T.; Neděla, V.; Heger, D. Vitrification and increase of basicity in between ice Ih crystals in rapidly frozen dilute NaCl aqueous solutions. *J. Chem. Phys.* **2019**, *151*, 014503. [CrossRef] [PubMed]
27. Angell, C.; Choi, Y. Crystallization and vitrification in aqueous systems. *J. Microsc.* **1986**, *141*, 251–261. [CrossRef]
28. Vozovyk, K.; Bobrova, O.; Prystalov, A.; Shevchenko, N.; Kuleshova, L. Amorphous state stability of plant vitrification solutions. *Biologija* **2020**, *66*, 47–53. [CrossRef]
29. Her, L.; Deras, M.; Nail, S. Electrolyte-Induced Changes in Glass Transition Temperatures of Freeze-Concentrated Solutes. *Pharm. Res.* **1995**, *12*, 768–772. [CrossRef]
30. Nesarikar, V.; Nassar, M. Effect of Cations and Anions on Glass Transition Temperatures in Excipient Solutions. *Pharm. Dev. Technol.* **2007**, *12*, 259–264. [CrossRef] [PubMed]
31. Ablett, S.; Izzard, M.; Lillford, P. Differential scanning calorimetric study of frozen sucrose and glycerol solutions. *J. Chem. Soc. Faraday Trans.* **1992**, *88*, 789. [CrossRef]
32. Zhao, L.; Pan, L.; Cao, Z.; Wang, Q. Confinement-induced vitrification of aqueous sodium chloride solutions. *Chem. Phys. Lett.* **2016**, *647*, 170–174. [CrossRef]

Disclaimer/Publisher's Note: The statements, opinions and data contained in all publications are solely those of the individual author(s) and contributor(s) and not of MDPI and/or the editor(s). MDPI and/or the editor(s) disclaim responsibility for any injury to people or property resulting from any ideas, methods, instructions or products referred to in the content.